Deepthi S Nair [1,2], *Jayasudha S* [3], *Ananda Kumar V. M,* [1,4]

[1] Postgraduate and Research Department of Physics, Mahatma Gandhi College, University of Kerala, Thiruvananthapuram, Kerala, 695004, India. [2] Department of Physics, Government College Kariavattom, Thiruvananthapuram, Kerala, 695581 India. [3] Department of Physics, HHMSPB NSS College for Women, Neeramankara, Thiruvananthapuram, Kerala, 695040, India. [4] Department of Physics, VTMNSS College Dhanuvachapuram, Thiruvananthapuram, Kerala,695003, India

Dual-mode environmental remediation of toxic dyes through chemo-catalytic and photocatalytic pathways using covellite (CuS) nanosheet clusters

ABSTRACT

Clusters of high-purity Covellite (CuS) nanosheets with remarkable catalytic properties were synthesized by a simple mechanochemical process, which effectively addressed certain pitfalls of traditional solid-state synthesis, including hours-long grinding, the necessity of annealing to remove byproducts, and the hurdles in achieving crystallite sizes below 20 nm. The study of reaction mechanisms revealed the formation of an intermediate [Cu(tu)] Cl. 0.5 H2O, which acted as a self-sacrificial precursor for forming CuS nanosheets. The extensive characterization incorporating XRD with Rietveld refinement, HRTEM, FESEM, EDS, UV-VIS absorption, FTIR, and Raman Spectroscopy confirmed the formation of phase pure hexagonal CuS with stacked sheet-like morphology forming microflowers, with an average crystallite size of 11nm and having an optical band gap of 1.91 eV. Studies on the degradation of Methyl Orange (MO), a major environmental pollutant, using Covellite nanosheets as a dual catalyst had demonstrated remarkable efficiency, achieving 84% degradation in 12 minutes through chemo-catalysis and 89.5% in 40 minutes through photocatalysis. This study suggests ecofriendly and promising dual pathways to eliminate organic dye contamination by employing Covellite(CuS) nanocatalyst.

__Keywords:__ Covellite(CuS), chemo-catalysis, photocatalysis, Methyl Orange (MO), Langmuir-Hinshelwood model

1. INTRODUCTION

The widespread application of synthetic dyes across industries like fabrics, paints, papers, and plastics results in the expulsion of toxic-colored effluents, contaminating the whole environment [1,2]. These dyes are well known for their resilience to deteriorate by conventional methods and their capability to invade various food chains, causing cancer and mutations [3]. Using nanostructure catalysts presents an advanced strategy for breaking down the toxic organic dye molecules in wastewater into benign molecules, offering a sophisticated solution for environmental amelioration [4].

Transition metal oxides like TiO_2, ZnO, and CuO have demonstrated their effectiveness as catalysts for degrading dyes in wastewater treatment [5- 7]. Among them, TiO_2 is particularly acclaimed for its widespread use in degrading dyes and pharmaceuticals in polluted wastewater. It has been utilized as a standalone photocatalyst and with other semiconductors to enhance its catalytic activity. However, these materials possess drawbacks like swift electron-hole recombination, wide band gaps, and limited absorption in the visible region [8]. In contrast, transition metal sulfide nanostructures demonstrate promising catalytic degradation of organic pollutants because of their significant reactivity at small concentrations, non-toxic nature, excellent chemical stability, remarkable electrical and optical properties, and suitable band gap characteristics [9,10]. Consequently, researchers have focused on investigating the photocatalytic capabilities of various metal sulfides such as CdS, ZnS, Bi_2S_3,

and CuS [10]. Among copper-based chalcogenides, particularly Covellite, copper monosulfide (CuS) is a highly versatile compound featuring size- and shape-tunable physical and chemical properties [11,12]. The inherent properties of CuS position it as a promising candidate for various applications across different fields, including photocatalysis, chemo-catalysis, lithium-ion batteries, solar cells, supercapacitors, and more [12-14]. CuS nanoparticles are attracting considerable interest as catalysts for dye degradation because of their distinct characteristics. Their large surface area and adjustable morphologies offer numerous active sites that facilitate catalytic reactions[15]. Moreover, the narrow bandgap of CuS enables efficient absorption of visible light, enhancing the photocatalytic breakdown of dye molecules into less toxic byproducts under ambient conditions. In contrast to many other metal sulfide catalysts, CuS nanoparticles are both cost-effective and chemically stable, making them ideal for repeated use in environmental remediation efforts[16,17].

In chemo-catalytic applications, CuS nanoparticles function as effective catalysts for various chemical reactions, such as hydrogenation, electron transfer, and reduction. Their high surface area and unique electronic structure promote efficient adsorption and activation of reactants, leading to enhanced reaction rates[18]. Moreover, in the realm of photocatalysis, CuS nanoparticles demonstrate promising potential for solar-driven environmental remediation and energy conversion processes. When exposed to light, CuS nanoparticles generate electron-hole pairs, which can initiate redox reactions on their surface or facilitate the degradation of organic pollutants in water or air [18-20]. Numerous studies have explored the use of CuS in degrading a range of hazardous dyes and chemicals. Bekhit et al. demonstrated that CuS nanorods synthesized via gamma radiolysis showed impressive chemo-catalytic performance, degrading methylene blue (MB) and Congo Red (CR) dyes in just 40 and 330 seconds, respectively, in the presence of sodium borohydride (NaBH$_4$)[18]. Shawky et al. also reported exceptional photocatalytic activity of urchin-like CuS nanostructures, which successfully degraded Malachite Green (MG) dye within 90 minutes[21]. CuS has been integrated into various composites for catalytic applications. Farooq M.H. et al. discovered that a CuS-TiO$_2$ composite, under solar irradiation, achieved significant photocatalytic efficiency, decolorizing 80% of MO dye in 80 minutes [22]. Moreover, Mohammed R. et al. utilized CuS QDs @ ZnO hybrid nanocomposite for the degradation of MB dye and certain

pharmaceuticals using solar simulations[23]. Consequently, CuS-based nanocatalysts offer a sustainable and efficient approach to address environmental pollution through the catalytic degradation of dyes. Thus, the application of CuS nanoparticles in both chemo-catalysis and photocatalysis holds excellent potential for mitigating the adverse environmental impacts of organic dye pollution, contributing to cleaner and healthier ecosystems.

The nanoparticles of CuS with a wide variety of morphologies, such as flakes, plates, rods, flowers, whiskers, hollow spheres, tubes, fibers, sheets, and urchin-like structures [24-26], have been reported so far. Many synthesis procedures are adopted for CuS nanostructures via solution chemistry, hydrothermal and solvothermal, sonochemical, hot injection, microwave irradiation, and solid-state routes [25-27]. Conventional solid-state synthesis involves grinding or milling the reactants, followed by annealing to remove by-products [28,29]. The method has the disadvantage of relatively long milling times and low yield. Annealing at high temperatures also generates aggregated particles with a broad size distribution. Most of the other room-temperature techniques produce low yields and require the selection of appropriate solvents, surfactants, or sophisticated instruments. Though solid-state synthesis of many oxides [29, 30] was reported earlier, the onset of phase transformation of Covellite at 200 ºC [31] limits the necessity of annealing for such synthesis. Thus, the room-temperature solid-state synthesis of Covellite with excellent catalytic efficiency illuminates a new pathway for environmental remediation by metal sulfide nanostructures.

Here, Covellite (CuS) nanosheets were prepared using a mechanochemical method at room temperature [32]. Exploring potential pathways for the synthesis of CuS nanoparticles, the structural, optical, vibrational, and morphological characterizations were also investigated. As far as we know, this is the first study to demonstrate the dual functionality of CuS nanosheets in the decomposition of methyl orange (MO) by two distinct approaches: in the presence of sodium borohydride (NaBH$_4$) and in the presence of sunlight.

2. MATERIALS AND METHODS

2.1. Materials

Copper Chloride Dihydrate (CuCl$_2$.2H$_2$O), Thiourea (CH$_4$N$_2$S), and Sodium Hydroxide (NaOH) pellets were all of the analytical grades and were used as obtained. De-ionized water served as the solvent, and absolute ethanol along
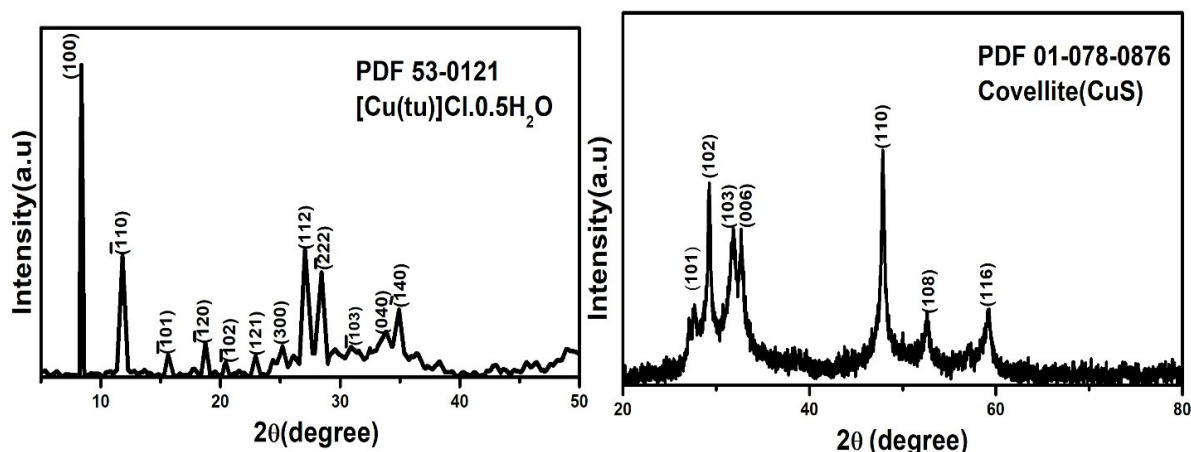
Figure 1: XRD patterns of [Cu(tu)]Cl. 0.5H$_2$O intermediate and Covellite nanosheets

with de-ionized water was used for washing throughout the entire process.

2.2. Synthesis of Covellite nanosheets

Mechanochemical synthesis of covellite was done by grinding copper chloride and thiourea in the molar ratio 1:2. When the mixture turned pale green, NaOH pellets were also added, and grinding was continued for five minutes until the mixture turned black. The black mixture was collected and washed several times using deionized water and absolute ethanol, then dried at 80ºC to obtain greenish-black CuS nanoparticles. To study the reaction mechanism, the pale green intermediate product, formed prior to the addition of NaOH, was separated, centrifuged many times, and oven-dried to obtain a white powder.

2.3. Characterization

The Bruker D8 Advance Diffractometer with CuKα Radiation was used to investigate the powder XRD pattern of the CuS. The UV-Visible absorption spectra and catalytic activities of the sample were recorded using a UV-Visible absorbance Spectrophotometer (Jasco-V-570) in the wavelength range of 200-800 nm. Energy Dispersive Analysis, i.e., EDS, was performed using Carl Zeiss EVO 18 Research Energy Dispersive X-RAY Analyser. Surface morphology was studied by Field Emission-SEM measurements using Nova NanoSEM-450(Model No.1027647, FEI, USA). The high-resolution TEM was carried out using Jeol/JEM 2100 instrument. The FTIR spectra of the samples were recorded using Thermoscientific Nicolet iS50 FTIR Spectrophotometer. Raman Spectroscopic studies were done using LabRAM Horiba Raman Spectrometer in the range 50-800cm^{-1}. The surface porous characteristics were investigated using a Quantachrome Instrument (Brunauer Emmett Teller Nova Touch lx4).

2.4. Chemo-Catalytic and Photocatalytic degradation studies

The chemo-catalytic and photocatalytic effects of prepared CuS nanostructure were determined by observing the color degradation of azo dye methyl orange (MO). For chemo-catalytic studies, various amounts of catalyst (0.5 mg, 1 mg, and 1.5 mg) were added to 20 ml 0.05 mM solution of MO containing 1 mg NaBH$_4$, and the absorption spectrum of the mixture was taken for each catalytic dosage until complete degradation. For photocatalytic experiments, various quantities of CuS catalyst(10,20 and 30 mg) were added to 100 ml 0.03 mM solution of MO.2 ml H$_2$O$_2$ (30 wt.%) was dropped into the reaction mixture and was stirred in the dark about 30 min to achieve adsorption-desorption equilibrium of the dye solution. The photocatalytic activity was determined under solar irradiation by analyzing the progress of decomposition of the dye at regular intervals of 10 min for each catalytic dosage using a UV-visible absorption spectrophotometer. The photocatalytic experiment was conducted under direct sunlight from 11 AM to 2 PM in February-March 2023.

3. RESULTS AND DISCUSSION

3.1. Structural analysis

The XRD patterns (Fig.1) of both the intermediate and final products were examined to elucidate the formation mechanism of CuS [eqns (1)-(3)]. The diffraction peaks of the intermediate formed by the reaction of thiourea with copper chloride can be indexed to the monoclinic phase (ICDD No. 53-0121) of [CuSC(NH$_2$)$_2$]Cl. 0.5 H$_2$O, i.e., [Cu(tu)]Cl. 0.5 H$_2$O [33].
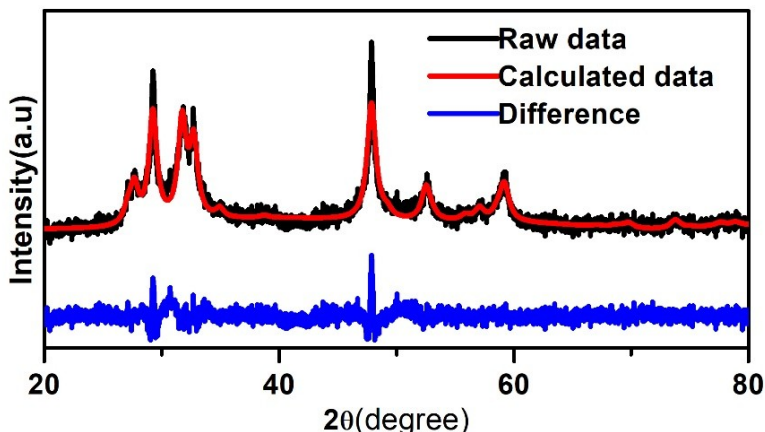
Figure 2: Rietveld refinement pattern of CuS
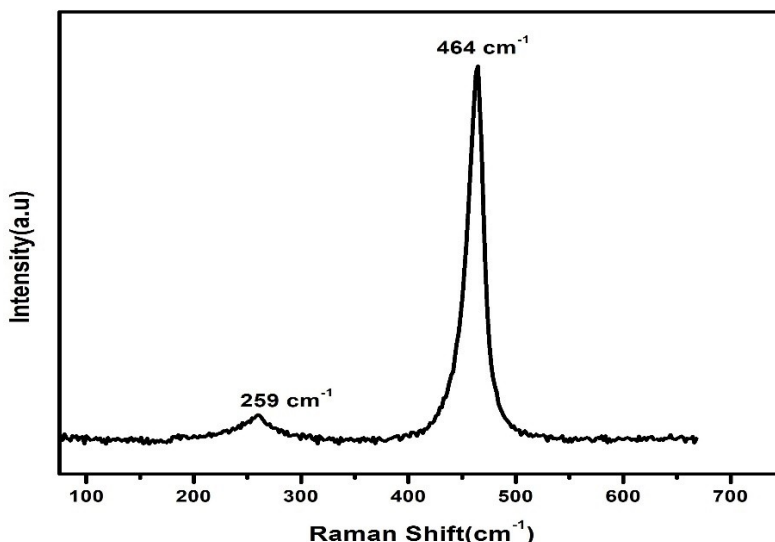
Figure 3: Raman spectrum of Covellite nanosheets

$$2CuCl_2 2H_2O + 2S = C(NH_2)_2 \rightarrow 2CuCl +$$
$$(SCNH_2NH)_2 + 2HCl \quad\quad (1)$$
$$CuCl + S = C(NH_2)_2 + 0.5H_2O \rightarrow$$
$$[CuSC(NH_2)_2]Cl . \ 0.5H_2O \quad\quad (2)$$
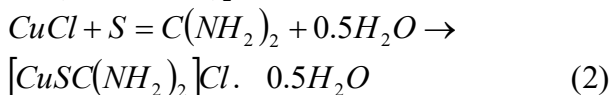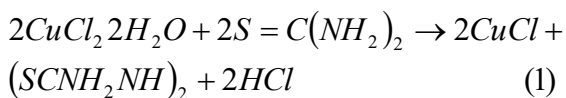
In the second grinding stage, the [Cu(tu)] Cl. $0.5H_2O$ intermediate acted like a self-sacrificial precursor, contributing Cu and S sources to create greenish-black Covellite nanoparticles [33] under alkaline conditions.

$$4[Cu(tu)]Cl \ 0.5H_2O + 4NaOH + O_2 + 4H_2O \rightarrow$$
$$4CuS + 8NH_3 + 4CO_2 + 4NaCl + 4H_2O \quad\quad (3)$$
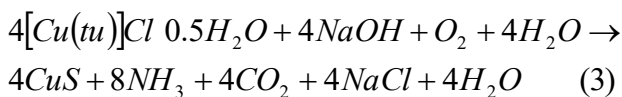
The 1:2 molar ratio of copper chloride to thiourea in the mechanochemical synthesis of covellite (CuS) is crucial for obtaining the desired copper monosulfide phase. This ratio provides an excess of thiourea, ensuring an adequate supply of sulfur to completely react with the copper ions and preventing the formation of unwanted phases such as Cu_2S or Cu1.8S [32,33]. The additional thiourea also increases the system's reactivity, facilitating the efficient production of high-quality greenish-black CuS nanoparticles through the complete sulfurization of copper under mechanochemical conditions. This synthesis method showcases impressive scalability, achieving a yield of about 97%. Conducted at room temperature and pressure, it can be easily scaled up for larger
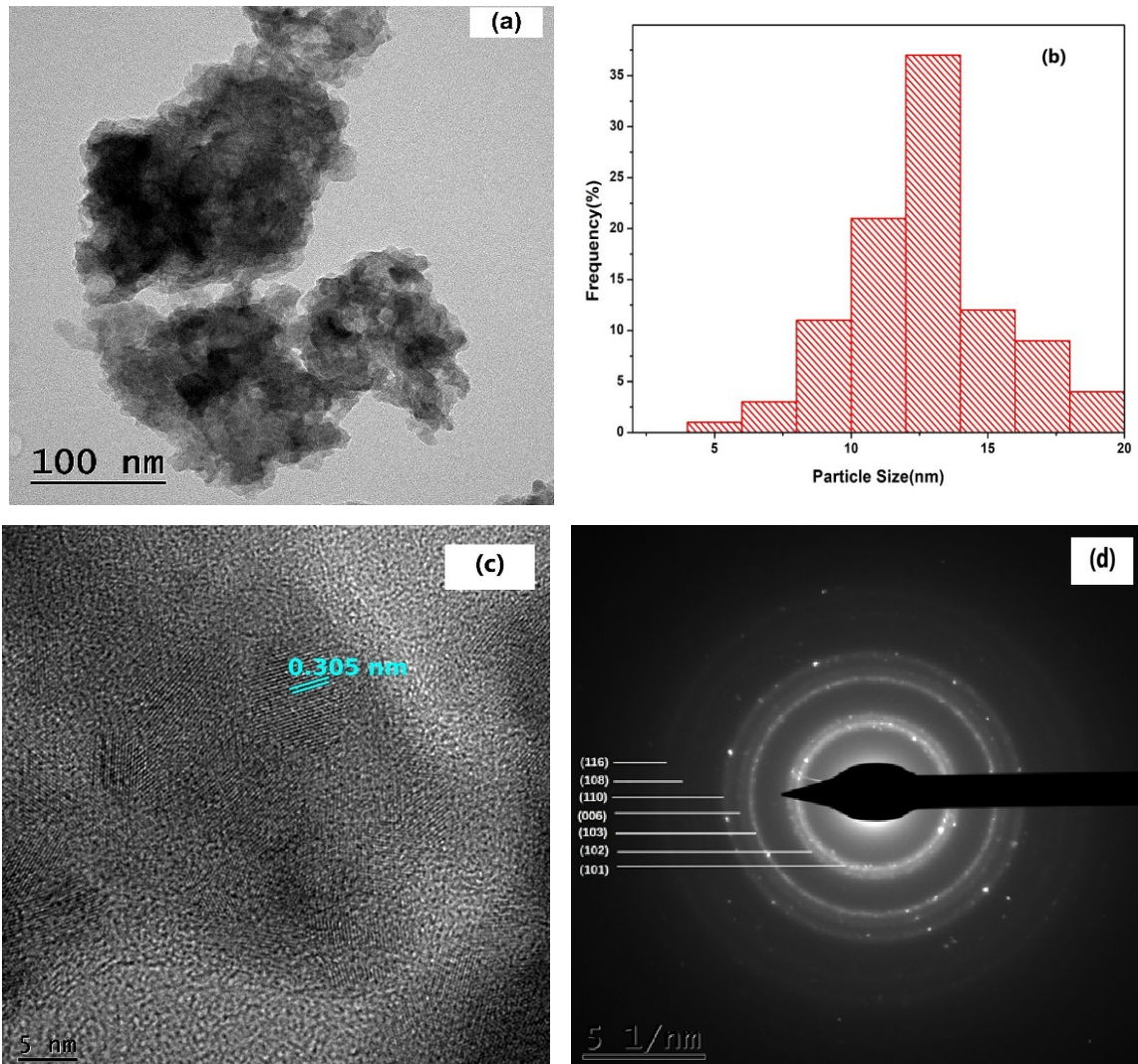
Figure 4*:TEM analysis of the sample (a) TEM image showing slightly aggregated particles (b) particle size distribution histogram revealing a mean particle size of 12.7 nm (c) HR-TEM image with an interplanar spacing 0.305 nm in agreement with (102) diffraction planes (d) selected area electron diffraction (SAED) pattern confirming the existence of (101), (102), (103), (006), (110), (108), and (116) planes corresponding to hexagonal CuS nanoparticles.*

batches, making it a cost-effective solution for large-scale production.

The XRD pattern for the prepared Covellite nanosheets shown in Fig.1 detects seven major peaks at 27.64º,29.23º, 31.6º, 32.64º, 47.84º,52.61º and 59.12º corresponding to (101), (102), (103), (006), (110), (108) and (116) lattice planes respectively, which corresponds to typical CuS (Covellite) with hexagonal structure (ICDD No:01-078-0876).

The (110) diffraction peak is comparatively stronger than the (103) peak, indicating the preferential orientation in the sample [34]. The crystallite size of the sample was assessed by the

Scherrer equation [35]: $D = \dfrac{K\lambda}{\beta cos\theta}$ (4)

where K is the shape factor(K=0.9), λ is the wavelength of the X-ray source in nm, θ is the diffraction angle, and β is the full width at half maximum (FWHM) in radians. As per the Scherrer equation, the crystallite size was evaluated as 11 nm.

Rietveld Refinement of the XRD pattern of the as-synthesized CuS sample was done with Diffract
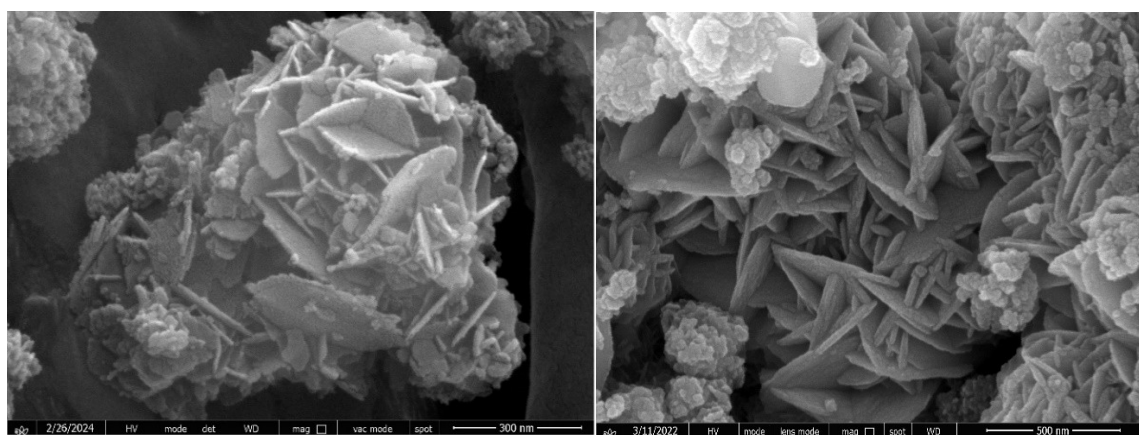
Figure 5: *FE-SEM images of Covellite nanosheets forming clusters with a micro-flower-like appearance*
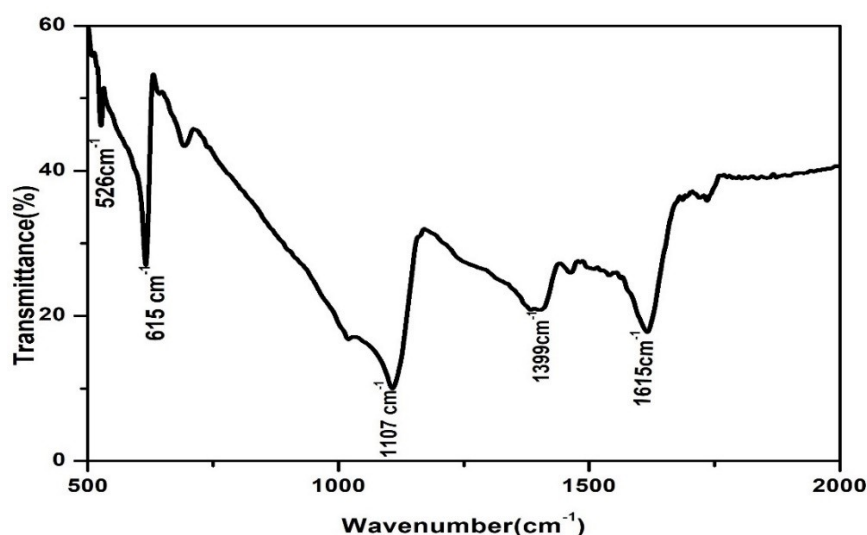
Figure 6: *FTIR spectrum of Covellite nanosheets*

Sute Plus -TOPAS software. The raw, computed, and difference data are plotted in Fig. 2. The space group used for the refinement was P63/mmc. The background was modeled by a Chebyshev polynomial of order 10, while the peak profiles were fitted using the Lorentzian function.

The sample crystallizes with the hexagonal structure, and the lattice constant values estimated as a result of refinement are a=3.80291 Å and c=16.4389 Å with R_{wp} value 6.22 and goodness of fit 1.52. The average crystallite size calculated from the refinement procedure is found to be 11 nm.

Structure and phase purity were confirmed using Raman Spectroscopy, shown in Fig.3, and exhibits two prominent peaks at 259 and 464 cm^{-1}. The strong one at 464 cm^{-1} can be due to the A_{1g} longitudinal optic (LO) mode of S-S stretching vibrations, and the diminished peak at 259 cm^{-1} is due to the A_{1g} transverse optic mode (TO) of CuS;

both are associated with the hexagonal phase of Covellite [36,37]. Like XRD, no additional peaks due to any impurity or other phases are observed. The TEM micrograph of CuS in Fig. 4(a) reveals nearly spherical and aggregated particles with a size distribution of 5.8 to 13.1 nm (Fig. 4(b)). The mean size of particles estimated is 12.7 nm and is in agreement with XRD analysis. The interplanar distance estimated for the sample (Fig. 4(c)) is 0.305 nm, in agreement with the (102) diffraction planes as evident from XRD. The diffraction pattern of the selected area, i.e., SAED ((Fig. 4(d)) reveals the polycrystalline nature of the sample, and the corresponding (hkl) planes are indexed as (101), (102), (103), (006), (110), (108), and (116) planes of hexagonal CuS nanoparticles.

Fig. 5 shows the FE-SEM micrographs of synthesized sample at different magnifications. It is obvious that the CuS nanoparticles exhibit an uneven distribution of sheet or plate-like structures
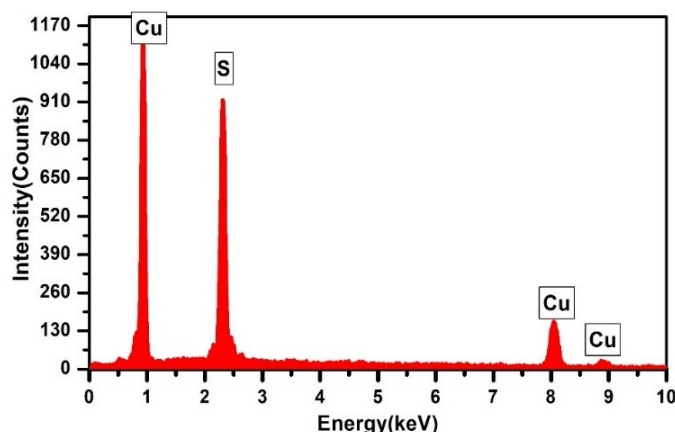
Figure 7:*EDS spectra of the Covellite nanosheets*

that are tightly bonded into clusters, forming micro-flowers. Unlike solution, where the diffusion rate of ions and nucleation are faster, mortar grinding in the current synthesis results in a paste-like environment, which prevents further diffusion and, hence, the creation of new nuclei [30,32]. As a result, the nuclei present would progressively develop into nanosheets over time. In the current amalgamation process, the manual grinding of the precursors could result in inconsistent blending, leading to non-uniform morphology. Consequently, this results in the appearance of flakes emerging into sheet-like structures, as in the FE-SEM image.

The FT-IR spectrum of the CuS sample is observed as in Fig. 6. The characteristic vibration peaks at 526 and 615 cm^{-1} can be assigned to disulfide(S-S) and Cu-S stretching vibrations, respectively [38,39]. The peak at 1615 cm^{-1} corresponds to the O-H bending of adsorbed water [40]. Also, the peaks corresponding to 1107 and 1399 cm^{-1} can be attributed to the C-N stretching mode and C=S bending mode of thiourea, respectively [40,41].

The quantitative analysis of the synthesized CuS nanosheets was revealed by EDS and shown in Fig. 7. Intense peaks of Copper and Sulfur are only observed with the atomic percentage nearly in the ratio 1:1 (Table. 1), suggesting pure Covellite phase.

Table 1:*EDS data of Covellite*

Element	Weight%	Atomic%
S	31.73	47.94
Cu	68.27	52.06
Total	100.00	100.00

The N_2 adsorption-desorption isotherm (Fig.8) reveals the surface textural analysis of synthesized nanosheets. The depicted isotherm appears to be type II-IV according to the IUPAC classification [42,43]. CuS nanosheets exhibited a specific surface area of about 6.95 m^2g^{-1}, a pore volume of 0.0258 ccg^{-1}, and an average pore diameter of 14.854 nm. The dual mode isotherm reveals non-homogenous pore distributions with micro and mesoporous structures and can be attributed to the typical morphology of the particle [42] suitable for catalytic applications. The specific surface area of the sample is comparable to earlier reports of CuS-based photocatalysts [43,44].
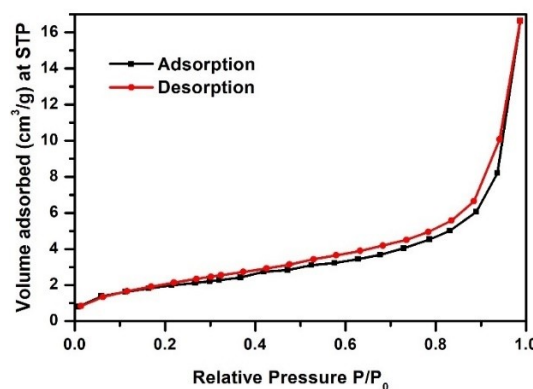
Figure 8: *N2 adsorption-desorption isotherm of Covellite nanosheets*

3.2. Optical Absorption

The UV-Visible absorption spectrum of the CuS sample is shown in Fig.9, which revealed two distinct absorptions, one in the UV-VIS region and the other extending to the near IR region. Both are blue-shifted compared to bulk. The vast band noticed in the UV-VIS region was assigned to the excitonic absorption in CuS, causing interband transitions [45,46], while that found at the near IR
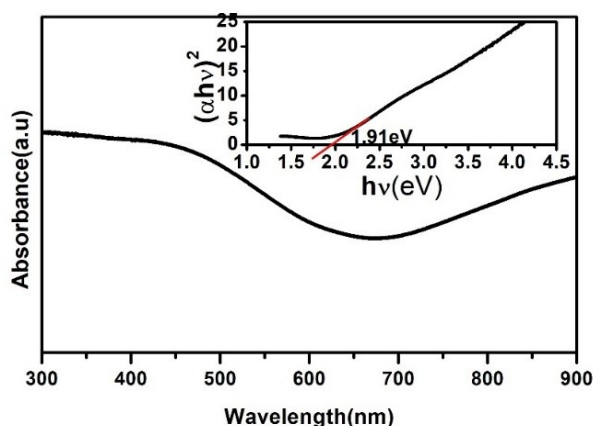
Figure 9: *UV-Visible absorption spectrum and Tauc plot(inset) of Covellite nanosheets*
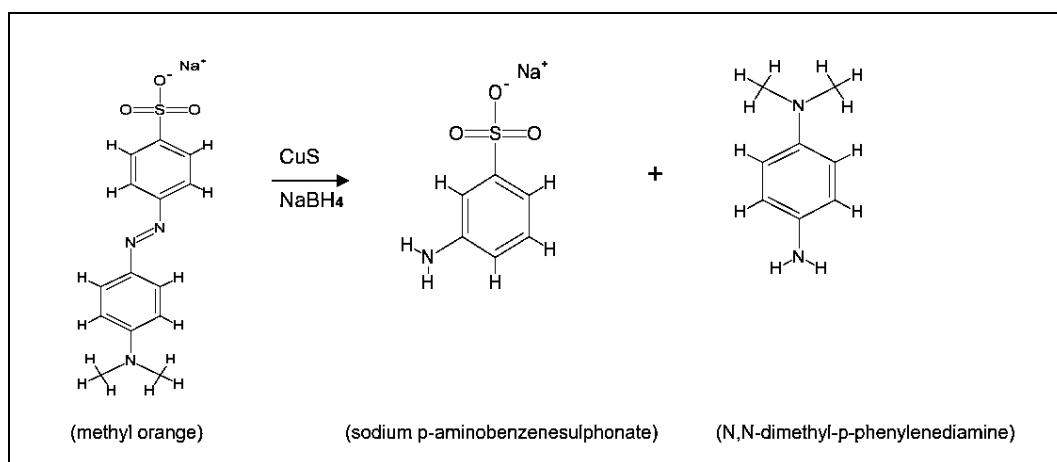
Figure 10: *Reduction of Methyl Orange with NaBH$_4$ through azo bond cleavage in the presence of CuS catalyst.*

region was as a result of localized Surface Plasmon Resonance (LSPR) and is a characteristic of covellite (CuS) [43-46]. The broad absorption of the prepared nanosheets in the visible region makes them a natural light harvester suitable for photocatalytic and solar cell applications.

Tauc's approach can be used to measure the direct band gap from the absorption spectrum as per the relation [47],

$$(\alpha h\nu) = A(h\nu - E_g)^n \qquad (5)$$

where $h\nu$ is the photon energy, α is the absorption coefficient, A is a constant, and E_g is the optical band gap energy of the material. Considering n=1/2 for direct transition, Tauc plot is drawn between $h\nu$ and $(\alpha h\nu)^2$, and the band gap of the Covellite nanostructure was calculated as 1.91eV, slightly greater than that of bulk CuS (1.85eV) [43].

3.3 Chemo-catalytic and Photocatalytic Activity

The chemo-catalytic efficacy of CuS nanostructures was determined in the reduction of an anionic dye, Methyl Orange (MO), using NaBH$_4$ as a reductant. The characteristic peaks of MO are at 464 nm due to the conjugated structure around the azo bond and at 280 nm due to the aromatic part. The CuS catalyst increases the rate of Hydrogen evolution from NaBH$_4$ and transfers the reducing species to dye molecules [48]. The schematic representation of the reduction of MO is shown in Fig.10.

The fast reduction is evident from the suppression of the major peak at 464 nm in the UV-Visible absorption spectrum within 12 minutes, as shown in Fig. 11(b)-11(d) for different amounts of CuS catalyst. Fig. 11(a) shows the absorption spectrum of MO reduction by NaBH$_4$ without catalyst recorded in 3-minute intervals up to 12
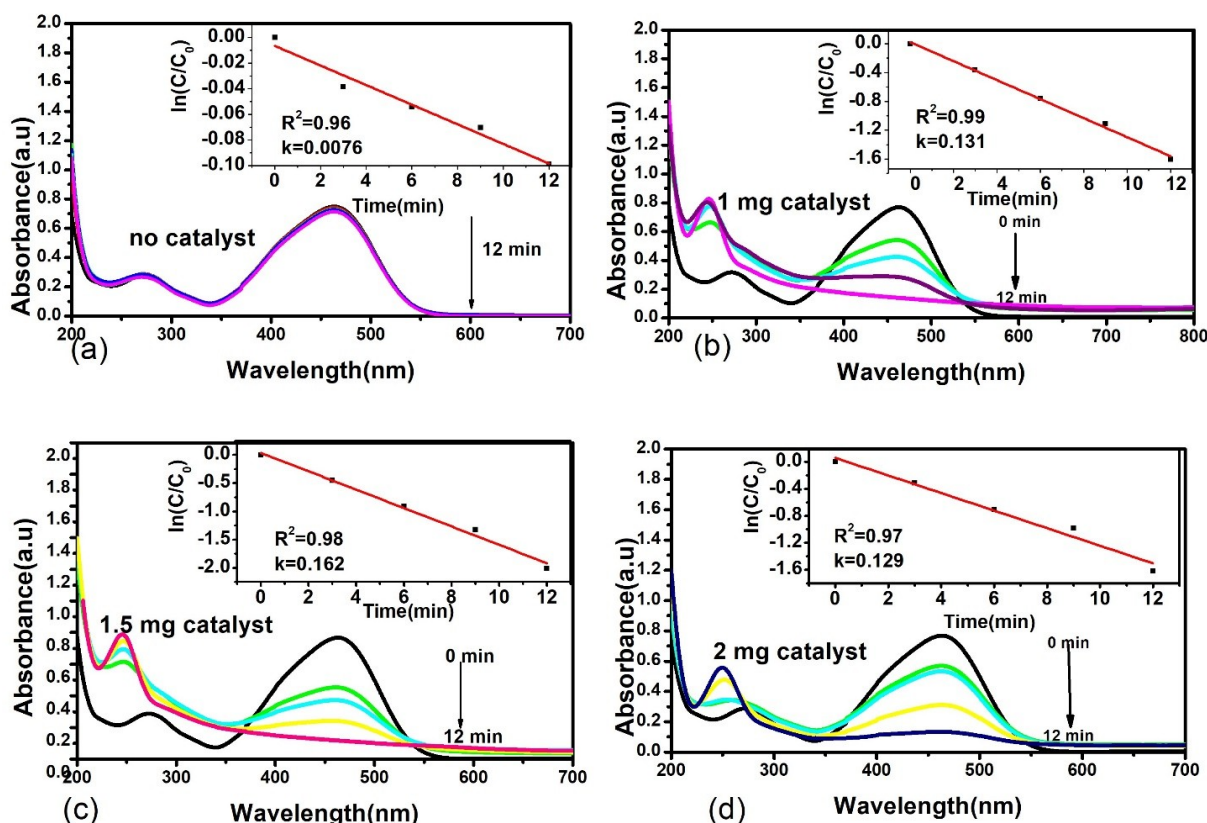
Figure 11: Catalytic degradation of MO dye by NaBH₄ recorded for a time span of 12 min (a) in the absence of Covellite (b) with 1 mg catalyst (c) with 1.5 mg catalyst (d) with 2 mg catalyst (each color represents absorption spectrum recorded at a particular time). Inset of each figure shows the respective linear plots of ln C/C₀ with time.

minutes. The slow variation in the peak intensity at 464 nm indicates the poor reduction reaction rate in the absence of the catalyst. The dye completely decolorizes and forms the hydrazine derivatives [48] within 12 min for 1 mg,1.5 mg, and 2 mg catalytic dosages and attains a steady state. The formation of the amino product, sodium p-aminobenzenesulphonate after reduction, is evident from the intensifying peak at 246 nm during the course of the reaction [49].

The reduction reactions of MO were performed without catalyst and in the presence of 1 mg, 1.5 mg, and 2 mg catalysts, and the percentage degradation is drawn as shown in Fig 12. The addition of 1 mg catalyst increased the degradation rate from 8.64% to 80.9%. When the amount of catalyst was increased from 1 mg to 1.5 mg, the degradation percentage reached 84%. However, for 2 mg catalyst dosage, the degradation rate decreased to 79%, which was due to the aggregation of the catalyst with time, which in turn reduces the active sites for the reactants. The linear correlation between ln (C/C₀) with the reaction time (t) denotes it is a pseudo-first-order

reaction in accordance with the Langmuir-Hinshelwood model [50,51] (inset of Fig. 11(a)-(d)) such that:

$$\ln\left(\frac{C}{C_0}\right) = -kt \qquad (6)$$

where C_0 represents the concentration at t=0 min, C stands for the concentration at a time t min, and k denotes the rate constant of the reaction. The rate constant obtained from the slope of the fitted straight line is found to increase from 7.6×10^{-3} min^{-1} for zero catalyst dosage to 1.3×10^{-1}, 1.6×10^{-1}, and 1.2×10^{-1} min^{-1} for 1 mg,1.5 mg, and 2 mg catalyst dosage respectively.

Here, the CuS nanosheets act as a platform for the adsorption of dye molecules. The BH_4^- anions in aqueous solution transfer electrons to dye molecules through the nanocatalyst, causing the reduction of dye. The high redox potential difference between electron donor (BH_4^-) and acceptor (MO molecules) hinders the direct electron transfer between them [48-50]. The electron transfer from BH_4^- ions to MO molecules
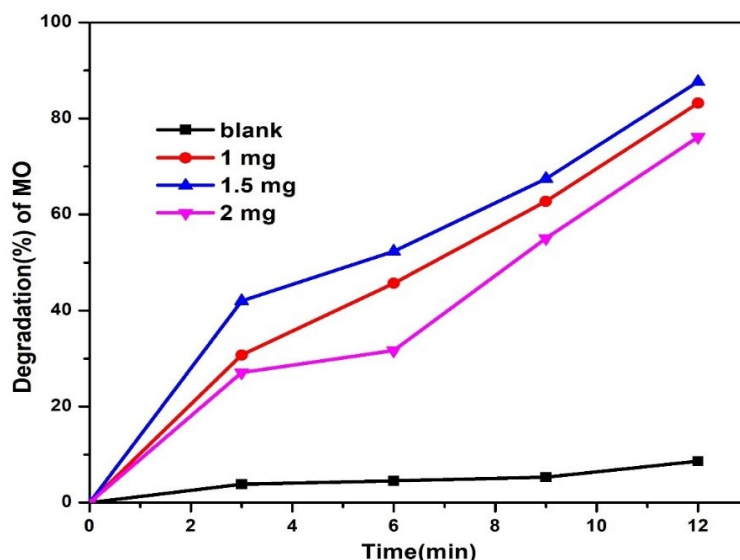
Figure 12: *Percentage degradation of MO dye by NaBH₄ in the absence and presence of 1 mg,1.5 mg, and 2 mg CuS catalyst*
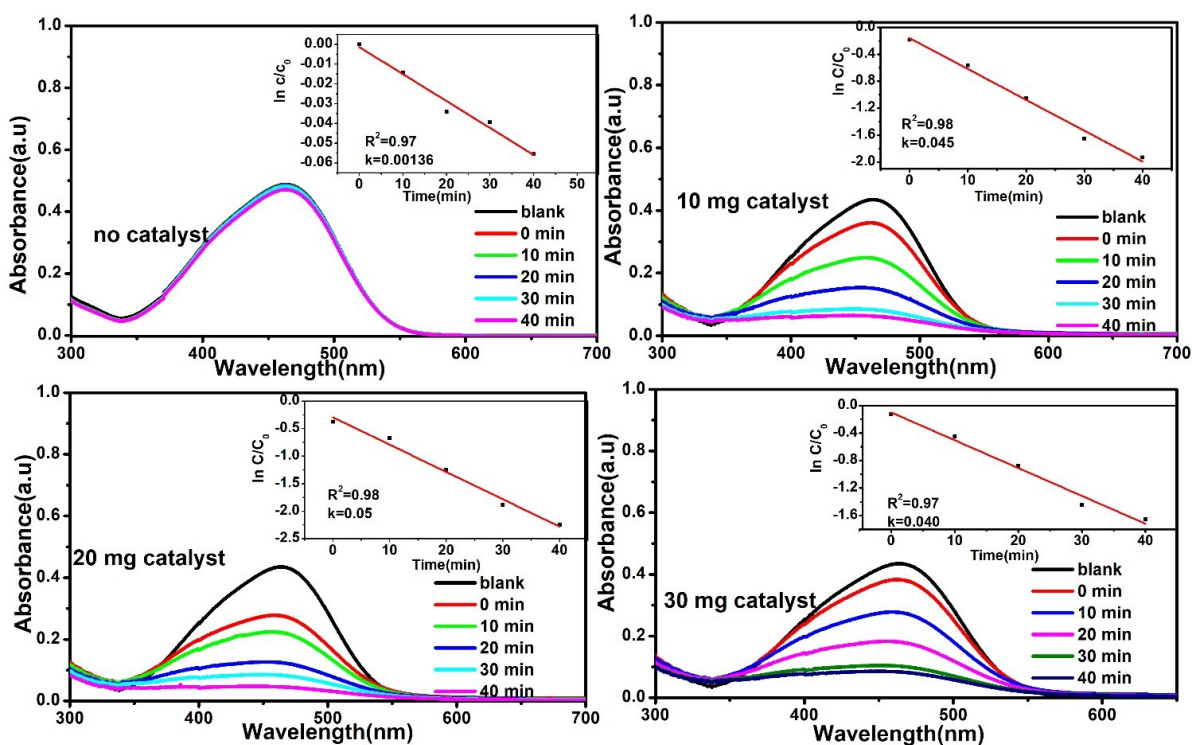
Figure 13: *Photo Catalytic degradation of MO dye recorded for an equal interval of 10 min up to 40 min (a)in the absence of Covellite catalyst(b) with 10 mg catalyst(c) with 20 mg catalyst(d) with 30 mg catalyst (each color represents absorption spectrum recorded at a particular time). Inset of each figure shows the respective linear plots of ln C/C₀ with time.*

occurs through the CuS nanosheets, resulting in azo bond cleavage in MO and forming aromatic amines [49,50] in a short span. The relevant mechanism can be explained as follows:

$$CuS + MO \rightarrow CuS - MO \qquad (7)$$

$$CuS - MO + BH_4 \rightarrow CuS + MO^- + BH_3 \qquad (8)$$

$$MO^- + BH_3 + H^+ \rightarrow reduced\ product \qquad (9)$$
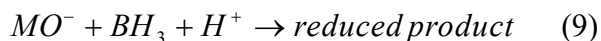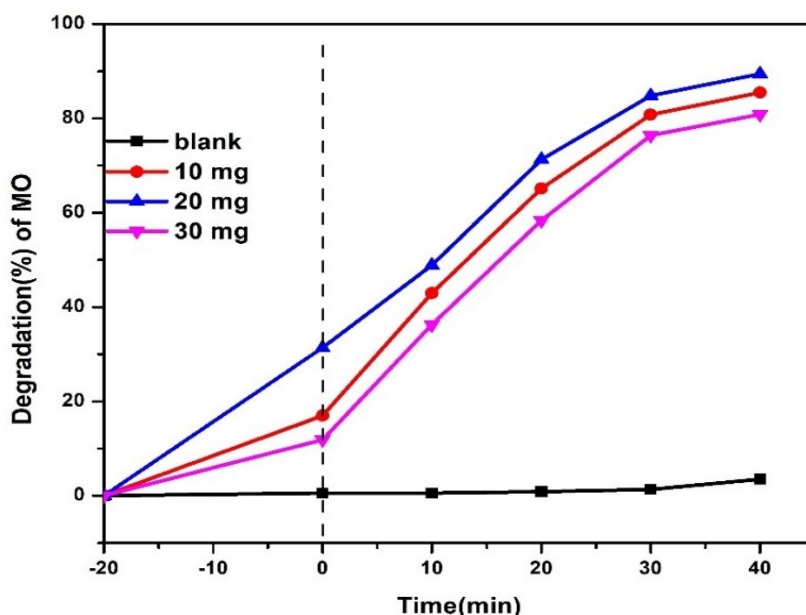
Figure 14: *Percentage degradation of MO dye in the absence and presence of 10 mg, 20 mg, and 30 mg CuS photocatalyst*
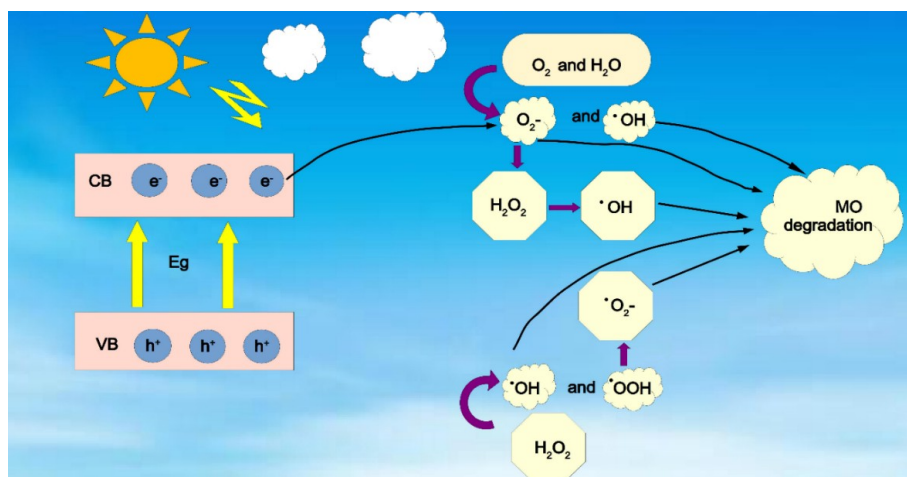
Figure 15: *Schematic representation of the mechanism of photo degradation of MO*

The photocatalytic performance of the CuS nano-catalyst was also analyzed by measuring the degradation of the 464 nm peak in the absorption spectrum of MO dye solution under solar light in the presence of H_2O_2 at regular intervals of 10 minutes. The degradation of MO in the absence and in the presence of 3 different catalytic dosages, such as 10 mg, 20 mg, and 30 mg, are studied (Fig. 13(a)-(d)).

The degradation percentage of MO at a specific time is shown in Fig. 14. In the absence of CuS, the blank experiment, under sunlight, revealed only minimal degradation, about 5.5% (even after 40 minutes). The addition of 10 mg catalyst resulted in a degradation of 85.49%, and 20 mg catalyst increased degradation to 89.5%, revealing that the photodegradation was definitely a photocatalytic reaction. As the catalytic dosage was increased to 30 mg, the degradation percentage decreased to 80.84% due to excessive CuS catalyst masking the photon transmission to the reaction mixture.

The photo-degradation was also in accordance with the pseudo-first-order kinetic reaction with a simplified Langmuir-Hinshelwood model [50-52] governed by the equation (6).

The rate constants calculated were 1.3×10^{-3} min^{-1} in the blank experiment, 4.5×10^{-2}, 5.0×10^{-2} and 4.0×10^{-2} min^{-1} for 10 mg, 20 mg, and 30 mg CuS dosage (inset of Fig.13(a)-13(d)), respectively.

Thus, 20 mg catalyst was found to be the optimum concentration for the current degradation study.

The photocatalytic degradation of methyl orange (MO) using CuS nanoparticles and hydrogen peroxide (H_2O_2) drops involves a series of chemical reactions[eqns (10)-(19)] [51-55] that are driven by the interaction of sunlight. When CuS nanoparticles absorb photons from the incident light, electrons in the nanoparticles are promoted to higher energy levels, creating electron-hole pairs. These charge carriers interact with dissolved oxygen and adsorbed water, generating Reactive Oxygen Species (ROS), $^{\bullet}O_2$ and $^{\bullet}OH$, which cause degradation of MO. The photocatalytic degradation mechanism is schematically represented in Fig.15.

$$CuS + h\nu \rightarrow CuS\left(e^- + h^+\right) \qquad (10)$$

$$H_2O \rightarrow H^+ + OH^- \qquad (11)$$

$$e^- + O_2 \rightarrow ^{\bullet}O_2^- \qquad (12)$$

$$h^+ + OH^- \rightarrow OH \qquad (13)$$
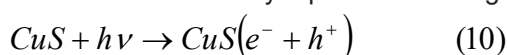
The H_2O_2 drops can effectively minimize the recombination of electron-hole pairs by trapping them to form ROS species and enhance the degradation process.

$$e^- + H_2O_2 \rightarrow ^{\bullet}OH + OH^- \qquad (14)$$

$$h^+ + H_2O_2 \rightarrow ^{\bullet}OOH + H^+ \qquad (15)$$

$$^{\bullet}OOH \rightarrow ^{\bullet}O_2^- + H^+ \qquad (16)$$
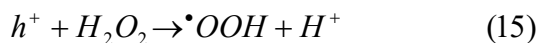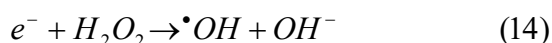
In addition, the accumulated electron in the CB can interact with $^{\bullet}O_2^-$ to form H_2O_2 that again can be reduced to $^{\bullet}OH$ [56].

$$e^- + ^{\bullet}O_2^- + 2H^+ \rightarrow H_2O_2 \qquad (17)$$

$$H_2O_2 \rightarrow 2^{\bullet}OH \qquad (18)$$
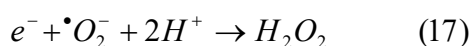
Then, the toxic organic dyes can be mineralized or converted to intermediates by the ROS through oxidation reactions.

$$MO + ^{\bullet}OH + ^{\bullet}O_2^- \rightarrow \text{degradation products} \quad (19)$$

In addition to creating ROS, the presence of H_2O_2 turns the pH of the solution environment to around 4. If the pH of the dye solution is lower than the Point of Zero Charge, i.e., PZC, of the catalyst, the surface charge at the surface of the CuS adsorbent becomes positive, and more anions are adsorbed [57]. Since the reported value of PZC of CuS is 5.2 [58], solution pH is 4, and MO is an anionic dye, better degradation was realized. Thus, the pH of the reaction mixture is also crucial for the current photodegradation study, including other factors like surface area and concentration of the catalyst.

CuS nanosheets, as catalysts, are not consumed in the reaction but facilitate the degradation process. The stability and reusability of the spent CuS catalyst (for the case of 20mg) are checked by filtering, washing, drying, and utilizing for successive cycles. It is found that degradation efficiencies in cycles 2 and 3 are 87.7% and 85.35%, respectively, which are only slightly lower than the first cycle (Fig.16). This indicates that CuS catalyst can be reused for multiple cycles of degradation. During the reuse of CuS nanoparticles, gradual catalyst mass loss may occur due to handling, washing, or filtration, leading to a reduced catalyst amount in subsequent cycles. This reduction, even in small amounts, can significantly impact degradation efficiency. To mitigate this, employing appropriate washing and regeneration methods, along with solvents like ethanol, can efficiently remove organic residues from the catalyst's surface, preserving active sites and ensuring sustained catalytic performance across multiple cycles.
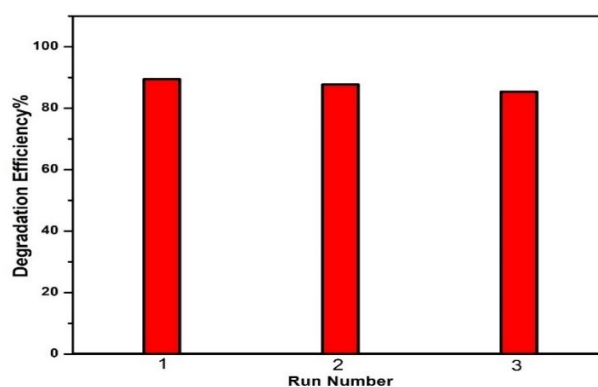
Figure 16: The recyclability of CuS nanosheets for three successive cycles of MO degradation

Thus, the synthesized Covellite (CuS) nanosheets can be effectively used both as a chemo-catalyst and photocatalyst for the degradation of Methyl Orange (MO) dye. Despite employing higher concentrations of MO and smaller catalyst quantities in the current study of chemo-catalysis compared to photocatalysis, the degradation of MO still proceeds relatively faster with higher rate constants in chemo-catalysis. Both degradation processes exhibit efficiencies above 80%, emphasizing the necessity for an optimal concentration of catalysts, as evident from Table 2.

The increased degradation rate of methyl orange in chemo-catalysis using sodium borohydride ($NaBH_4$) compared to photocatalysis using CuS nanoparticles under visible light is due

Table 2: *Summary of current catalytic and photo catalytic degradation study*

	Chemocatalysis (12 min)			Photocatalysis (40 min)		
Reaction Mixture (MO)	20ml 0.05mM			100ml 0.03mM		
Amount of CuS	1 mg	1.5 mg	2 mg	10 mg	20mg	30mg
Degradation Efficiency(%)	80.9	84.0	79.1	85.4	89.5	80.8
Rate constant (min^{-1})	1.3×10^{-1}	1.6×10^{-1}	1.2×10^{-1}	4.5×10^{-2}	5×10^{-2}	4×10^{-2}

Table 3: *Representative studies on MO degradation using CuS-based nano-catalysts*

Catalyst	Synthesis Method	Mass of Catalyst	Pollutant (MO) Conc.	Catalytic condition	Time (min)	Degradation (%)	Reference
CuS Microspheres	Solution aerosol thermolysis	0.10 g	3×10^{-5} M *MO+1ml* H_2O_2	VIS 300W *Xe Lamp*	45	50%	[56,11]
CuS Nanotubes	Hydrothermal	60 mg	100 ml MO	UV 20 W Hg lamp	140	91.5%	[59]
Starch Capped Cus NPs	Precipitation method	25 mg	50 ml 2×10^{-5} M MO+NaSO$_3$	Dark	20	78.3%	[38]
CuS Flower	Hydrothermal	30 mg	50 ml 10 mg/L MO	VIS 500 W Xe lamp	150	30%	[60]
CuS 3D Flower	Solvothermal	10 mg	10 ppm	300 W Xe lamp	60	34%	[61]
CuS NPs	Hydrothermal	0.05 g	20 mg/L MO	Sunlight	80	60%	[22]
CuS nano-spheres	Microwave irradiation	-	-	NaBH$_4$	10	80%	[62]
CuS Nano-Sheets	Mechano-chemical (grinding)	1.5 mg	1.65 mg MO in 100 ml 1 mg MO in Sunlight 100 ml+2 ml H$_2$O$_2$	NaBH$_4$ *Sunlight*	12 40	84% 89.5%	This Work

to several factors. In chemo-catalysis, NaBH$_4$ directly donates hydride ions to the dye molecules, leading to a fast and efficient reduction process. This is a simpler and quicker reaction compared to photocatalysis, which requires the absorption of light by CuS to generate electron-hole pairs. These charge carriers then create reactive oxygen species (ROS) that degrade the dye in a slower, multistep process. Additionally, chemo-catalysis

benefits from the strong reducing power of $NaBH_4$, while photocatalysis is limited by factors like light intensity, charge recombination, and the slower generation of ROS. Therefore, chemo-catalysis completes the degradation in a much shorter time due to its more direct reaction pathway.

This report demonstrates the efficacy of Covellite (CuS) nanosheets as both a chemo-catalyst and photocatalyst in degrading anionic MO dye, which is relatively underexplored compared to the cationic dye, Methylene Blue (MB), having a swifter degradation [11]. However, comparing what has been reported so far in previous studies (Table 3), it is clear that the synthesized Covellite nanosheet clusters exhibit enhanced chemo-catalytic and photocatalytic activities against Methyl Orange (MO) dye. The unique structure of the covellite nanosheets, produced via a simple and scalable mechanochemical process, notably improves their catalytic efficiency by offering a significant surface area and numerous active sites for reactions. Their chemo-catalytic performance is enhanced by their ability to promote rapid electron transfer, while the narrow bandgap of CuS boosts their photocatalytic activity by enabling efficient visible light absorption and generating reactive oxygen species (ROS). The high performance can be attributed to their small size, sheet-like morphology, and wide absorption range in the visible region.

4. CONCLUSION

Clusters of Covellite nanosheets were successfully synthesized through a simple mechanochemical process, offering benefits such as the exclusion of surfactants and the calcination process, reduced processing time, and a solution-free environment. XRD with refinement, Raman Spectroscopy, HR-TEM, and FE-SEM analysis confirmed the formation of phase pure ultra-small CuS nanoparticles having sheet-like morphology with uneven distribution. Covellite (CuS) nanosheets exhibit exceptional sunlight-driven and $NaBH_4$-driven catalytic activity in the degradation of Methyl Orange (MO) dye. To our current understanding, this is the first report unveiling the dual functionality of CuS nanosheets as a chemo-catalyst (in the presence of $NaBH_4$) and a photocatalyst (under visible light), enabling the efficient degradation of environmental contaminant Methyl Orange (MO). The degradation efficiency reached 84% within 12 min for chemo-catalysis and 89.5% after 40 min for photocatalysis by optimizing the amount of CuS catalyst. The enhanced catalytic performance can be credited to the synergistic effects of reduced crystallite size, sheet-like morphology, increased surface area, and the ability to harness a substantial portion of

sunlight. This work highlights a prospective and secure approach of utilizing Covellite (CuS) nano-catalysts to mitigate environmental pollution stemming from the dye industry.

REFERENCES

[1] J. Ahmed, A. Thakur, A. Goyal (2021) Industrial Wastewater and Its Toxic Effects. In Biological Treatment of Industrial Wastewater., p.1-14. https://doi.org/10.1039/9781839165399-00001

[2] M. Ilyas, W. Ahmad, H. Khan, S. Yousaf, M. Yasir, A. Khan (2019) Environmental and health impacts of industrial wastewater effluents in Pakistan: A review. Reviews on Environmental Health, 34(2), 171-186. https://doi.org/10.1515/reveh-2018-0078

[3] B. Lellis, C.Z. Fávaro-Polonio, J. Pamphile, J. Polonio (2019) Effects of textile dyes on health and the environment and bioremediation potential of living organisms. Biotechnology Research and Innovation, 3(2), 275-290. https://doi.org/10.1016/j.biori.2019.09.001

[4] A. Yaqoob, T. Parveen, K. Umar, M. Ibrahim (2020) Role of nanomaterials in the treatment of wastewater: A review. Water (Switzerland), 12(2), 495-507. https://doi.org/10.3390/w12020495

[5] K.P. Gopinath, N.V. Madhav, A. Krishnan, R. Malolan, G. Rangarajan (2020) Present applications of titanium dioxide for the photocatalytic removal of pollutants from water: A review. Journal of Environmental Management, 270,110906. https://doi.org/10.1016/j.jenvman.2020.110906

[6] A.K. Sibhatu, G.K. Weldegebrieal, S. Sagadevan, N.N. Tran, V. Hessel (2022) Photocatalytic activity of CuO nanoparticles for organic and inorganic pollutants removal in wastewater remediation. Chemosphere, 300, 134623. https://doi.org/10.1016/j.chemosphere.2022.134623

[7] O.E. Baibara, M.V. Radchenko, V.A. Karpyna, A.I. Levtushenko (2021) A review of some aspects for the development of ZnO-based photocatalysts for a variety of applications. Physics and Chemistry of Solid State, 22(3), 585-594. https://doi.org/10.15330/PCSS.22.3.585-594

[8] A.V. Nimmy, A. Mahesh, V.M. Anandakumar, V. Biju (2024) Revealing the role of defect-induced trap levels in sol–gel-derived TiO2 samples and the synergistic effect of a mixed phase in photocatalytic degradation of organic pollutants. Journal of Physics and Chemistry of Solids,185, 111774. https://doi.org/10.1016/j.jpcs.2023.111774

[9] M.B. Tahir, M. Rafique, M.S. Rafique, N. Fatima, Z. Israr (2020). Metal oxide-and metal sulfide-based nanomaterials as photocatalysts. In Nanotechnology and Photocatalysis for

Environmental Applications, p.77-96. https://doi.org/10.1016/b978-0-12-821192-2.00006-1

[10] D. Ayodhya, G. Veerabhadram (2018) A review on recent advances in photodegradation of dyes using doped and heterojunction based semiconductor metal sulfide nanostructures for environmental protection. Materials Today Energy, 9, 83-113. https://doi.org/10.1016/j.mtener.2018.05.007

[11] L. Isac, C. Cazan, L. Andronic, A. Enesca (2022) CuS-based nanostructures as catalysts for organic pollutants photodegradation. Catalysts, 12(10), 1135. https://doi.org/10.3390/catal12101135

[12] P. Roy, S.K. Srivastava (2015) Nanostructured copper sulfides: synthesis, properties and applications. CrystEngComm, 17(41), 7801-7815. https://doi.org/10.1039/c5ce01304f

[13] H. Ding, J. Yong, J. Zhang, B. Chen, B. Ding, X. Wang (2022) Anchoring Pd nanoparticles on hollow CuS nanoparticles for enhanced NIR-induced photothermal effects for chemotherapeutic drug delivery and gastric cancer treatment. Ceramics International, 48(11), 16085-16090. https://doi.org/10.1016/j.ceramint.2022.02.154

[14] G. Kalimuldina, A. Nurpeissova, A. Adylkhanova, D. Adair, I. Taniguchi, Z. Bakenov (2020) Morphology and dimension variations of copper sulfide for high-performance electrodes in rechargeable batteries: A review. ACS Applied Energy Materials, 3(12),11480-11499. https://doi.org/10.1021/acsaem.0c01686

[15] A. Sudhaik, P. Raizada, S. Rangabhashiyam, A. Singh, V.H. Nguyen, Q.V. Le, P. Singh (2022). Copper sulfides-based photocatalysts for degradation of environmental pollution hazards: A review on the recent catalyst design concepts and future perspectives. Surfaces and Interfaces, 33, 102182. https://doi.org/10.1016/j.surfin.2022.102182

[16] F. Jamal, A. Rafique, S. Moeen, J. Haider, W. Nabgan, A. Haider, M. Maqbool (2023) Review of metal sulfide nanostructures and their applications. ACS Applied Nano Materials, 6(9), 7077-7106. https://doi.org/10.1021/acsanm.3c00417

[17] N. Ul Ain, A. Aamir, Y. Khan, M.U. Rehman, D.J. Lin (2020) Catalytic and photocatalytic efficacy of hexagonal CuS nanoplates derived from copper (II) dithiocarbamate. Materials Chemistry and Physics, 242, 122408. https://doi.org/10.1016/j.matchemphys.2019.122408

[18] M. Bekhit, A.O. Abo El Naga, M. El Saied, M.I. Abdel Maksoud (2021) Radiation-induced synthesis of copper sulfide nanotubes with improved catalytic and antibacterial activities. Environmental Science and Pollution Research, 28, 44467-44478. https://doi.org/10.1007/s11356-021-13482-9

[19] F. Siddique, M.A. Rafiq, M.F. Afsar, M.M. Hasan, M.M. Chaudhry (2018) Enhancement of degradation of mordant orange, safranin-O, and acridine orange by CuS nanoparticles in the presence of H_2O_2 in dark and in ambient light. Journal of Materials Science: Materials in Electronics, 29, 19180-19191. https://doi.org/10.1007/s10854-018-0044-7

[20] C. Nethravathi, J.T. Rajamathi, M. Rajamathi (2019) Microwave-assisted synthesis of porous aggregates of CuS nanoparticles for sunlight photocatalysis. ACS Omega, 4(3), 4825-4831. https://doi.org/10.1021/acsomega.8b03288

[21] A. Shawky, S.M. El-Sheikh, A. Gaber, S.I. El-Hout, I.M. El-Sherbiny, A.I. Ahmed (2020) Urchin-like CuS nanostructures: simple synthesis and structural optimization with enhanced photocatalytic activity under direct sunlight. Applied Nanoscience, 10(7), 2153-2164. https://doi.org/10.1007/s13204-020-01283-4

[22] M.H. Farooq, I. Aslam, A. Shuaib, H.S. Anam, M. Rizwan, Q. Kanwal (2019) Band gap engineering for improved photocatalytic performance of CuS/TiO2 composites under solar light irradiation. Bulletin of the Chemical Society of Ethiopia, 33(3), 561-571. https://doi.org/10.4314/bcse.v33i3.16

[23] R. Mohammed, M.E.M. Ali, E. Gomaa, M. Mohsen (2022) Copper sulfide and zinc oxide hybrid nanocomposite for wastewater decontamination of pharmaceuticals and pesticides. Scientific Reports, 12(1), 18153. https://doi.org/10.1038/s41598-022-22795-9

[24] S.K. Nath, P.K. Kalita (2021) Temperature-dependent structural, optical, and electrical properties of CuS nanorods in aloe vera matrix. Nano-Structures & Nano-Objects, 25, 100651. https://doi.org/10.1016/j.nanoso.2020.100651

[25] R. Kushwah, A. Singh, A. Anshul, D. Mishra, S. S. Amritphale (2017) Facile and controlled synthesis of copper sulfide nanostructures of varying morphology. Journal of Materials Science: Materials in Electronics, 28,5597–5602. https://doi.org/10.1007/s10854-016-6227-1

[26] F. Goel, W. Chen, W. Cai (2014) Synthesis and biomedical applications of copper sulfide nanoparticles: from sensors to theranostics. Small ,10(4), 631–645. https://doi.org/10.1002/smll.201301174

[27] N. ul Ain, J. A. Nasir, Z. Khan, I. S. Butler, Z. Rehman (2022) Copper sulfide nanostructures: Synthesis and biological applications. RSC Advances, 12(12), 7550-7567. https://doi.org/10.1039/d1ra08414c

[28] J. Vasudevan, S. J. Jeyakumar, B. Arunkumar, M. Jothibas, A. Muthuvel, S. Vijayalakshmi (2022) Optical and magnetic investigation of Cu doped ZnO nanoparticles synthesized by solid state method. Materials Today: Proceedings, 48, 438-442. https://doi.org/10.1016/j.matpr.2020.12.429

[29] I. Khaldari, M. R. Naghavi, E. Motamedi (2021) Synthesis of green and pure copper oxide nanoparticles using two plant resources via solid-state route and their phytotoxicity assessment. RSC Advances, 11(6), 3346-3353. https://doi.org/10.1039/d0ra09924d

[30] T. Tsuzuki (2021) Mechanochemical synthesis of metal oxide nanoparticles. Communications Chemistry, 4(1),143. https://doi.org/10.1038/s42004-021-00582-3

[31] A. Narjis, A. Outzourhit, A. Aberkouks, M. El Hasnaoui, L. Nkhaili (2018) Spectroscopic study and thermoelectric properties of a mixed phase copper sulfide lamellas. Journal of Alloys and Compounds, 762, 46-48. https://doi.org/10.1016/j.jallcom.2018.05.183

[32] Y. Qin, X. Kong, D. Lei, X. Lei. (2018) Facial grinding method for synthesis of high-purity CuS nanosheets. Industrial & Engineering Chemistry Research, 57(8), 2759-2764. https://doi.org/10.1021/acs.iecr.7b04616

[33] J. Mao, Q. Shu, Y. Wen, H. Yuan, D. Xiao, M. M. Choi. (2009) Facile fabrication of porous CuS nanotubes using well-aligned [Cu (tu)] Cl· 1/2H$_2$O nanowire precursors as self-sacrificial templates. Crystal Growth and Design, 9(6), 2546-2548. https://doi.org/10.1021/cg8006052

[34] S. S. T. Selvi, J. M. Linet, S. Sagadevan (2018) Influence of CTAB surfactant on structural and optical properties of CuS and CdS nanoparticles by hydrothermal route. Journal of Experimental Nanoscience, 13(1), 130-143. https://doi.org/10.1080/17458080.2018.1445306

[35] B. D. Cullity (1956) Elements of X-ray Diffraction. Addison-Wesley Publishing.

[36] C. G. Munce, G. K. Parker, S. A. Holt, G. A. Hope (2007) A Raman spectroelectrochemical investigation of chemical bath deposited CuxS thin films and their modification. Colloids and Surfaces A: Physicochemical and Engineering Aspects, 295(1-3), 152-158. https://doi.org/10.1016/j.colsurfa.2006.08.045

[37] T. Safrani, J. Jopp, Y. Golan (2013) A comparative study of the structure and optical properties of copper sulfide thin films chemically deposited on various substrates. RSC Advances, 3(45), 23066-23074. https://doi.org/10.1039/c3ra42528b

[38] I. Savarimuthu, M. J. A. M. Susairaj (2022) CuS nanoparticles trigger sulfite for fast degradation of organic dyes under dark conditions. ACS Omega, 7(5), 4140-4149. https://doi.org/10.1021/acsomega.1c05697

[39] Z. Q. Mamiyev, N. O. Balayeva (2016) CuS nanoparticles synthesized by a facile chemical route under different pH conditions. Mendeleev Communications, 26(3), 235-237. https://doi.org/10.1016/j.mencom.2016.05.004

[40] J. P. Tailor, S. H. Chaki, M. P. Deshpande (2021) Comparative study between pure and manganese doped copper sulphide (CuS) nanoparticles. Nano Express, 2(1), 010011. https://doi.org/10.1088/2632-959X/abdc0d

[41] J. Zou, J. Zhang, B. Zhang, P. Zhao, X. Xu, J. Chen, K. Huang (2007) Synthesis and characterization of copper sulfide nanocrystal with three-dimensional flower-shape. Journal of

[42] Materials Science, 42, 9181-9186. https://doi.org/10.1007/s10853-007-1923-0

[42] S. Brunauer, L. S. Deming, W. E. Deming, E. Teller (1940) On a theory of the van der Waals adsorption of gases. Journal of the American Chemical Society, 62(7), 1723-1732. https://doi.org/10.1021/ja01864a025

[43] M. Pal, N. R. Mathews, E. Sanchez-Mora, U. Pal, F. Paraguay-Delgado, X. Mathew (2015) Synthesis of CuS nanoparticles by a wet chemical route and their photocatalytic activity. Journal of Nanoparticle Research, 17, 1-12. https://doi.org/10.1007/s11051-015-3103-5

[44] Z. Hosseinpour, A. Alemi, A. A. Khandar, X. Zhao, Y. Xie (2015) A controlled solvothermal synthesis of CuS hierarchical structures and their natural-light-induced photocatalytic properties. New Journal of Chemistry, 39(7), 5470-5476. https://doi.org/10.1039/c4nj02298j

[45] S. Adhikari, D. Sarkar, G. Madras (2017) Hierarchical design of CuS architectures for visible light photocatalysis of 4-chlorophenol. ACS Omega, 2(7), 4009-4021. https://doi.org/10.1021/acsomega.7b00669

[46] M. Basu, R. Nazir, P. Fageria, S. Pande (2016) Construction of CuS/Au heterostructure through a simple photoreduction route for enhanced electrochemical hydrogen evolution and photocatalysis. Scientific Reports, 6(1), 34738. https://doi.org/10.1038/srep34738

[47] M. Saranya, C. Santhosh, R. Ramachandran, P. Kollu, P. Saravanan, M. Vinoba, ... A. N. Grace (2014) Hydrothermal growth of CuS nanostructures and its photocatalytic properties. Powder Technology, 252, 25-32. https://doi.org/10.1016/j.powtec.2013.10.031

[48] A. Rajan, V. Vilas, D. Philip. (2015) Studies on catalytic, antioxidant, antibacterial and anticancer activities of biogenic gold nanoparticles. Journal of Molecular Liquids, 212, 331-339. https://doi.org/10.1016/j.molliq.2015.09.013

[49] A. Rahmani, H. Rahmani, A. Zonouzi (2018) Cu (BDC) as a catalyst for rapid reduction of methyl orange: room temperature synthesis using recycled terephthalic acid. Chemical Papers, 72, 449-455.

https://doi.org/10.1007/s11696-017-0297-2

[50] N. Sreeju, A. Rufus, D. Philip (2017) Studies on catalytic degradation of organic pollutants and anti-bacterial property using biosynthesized CuO nanostructures. Journal of Molecular Liquids, 242, 690-700. https://doi.org/10.1016/j.molliq.2017.07.077

[51] U. S. Udayachandran Thampy, A. Mahesh, K. S. Sibi, I. N. Jawahar, V. Biju (2019) Enhanced photocatalytic activity of ZnO–NiO nanocomposites synthesized through a facile sonochemical route. SN Applied Sciences, 1, 1-15. https://doi.org/10.1007/s42452-019-1426-z

[52] K. Kannan, D. Radhika, M. P. Nikolova, K. K. Sadasivuni, H. Mahdizadeh, U. Verma (2020)

Structural studies of bio-mediated NiO nanoparticles for photocatalytic and antibacterial activities. Inorganic Chemistry Communications, 113, 107755. https://doi.org/10.1016/j.inoche.2019.107755

[53] Y. Subramanian, A. Dhanasekaran, L. A. Omeiza, M. R. Somalu, A. K. Azad (2023) A review on heteroanionic-based materials for photocatalysis applications. Catalysts, 13(1), 173. https://doi.org/10.3390/catal13010173

[54] S. L. Zhou, L. G. Gong, X. Y. Zhao, Q. L. Liang, W. J. Zhang, L. Y. Wang, ... B. B. Zhou (2020) Synthesis and photocatalytic performance of copper sulfide by a simple solvothermal method. Chemical Physics Letters, 759, 138034. https://doi.org/10.1016/j.cplett.2020.138034

[55] W. Xu, S. Zhu, Y. Liang, Z. Li, Z. Cui, X. Yang, A. Inoue (2015) Nanoporous CuS with excellent photocatalytic property. Scientific Reports, 5(1), 18125. https://doi.org/10.1038/srep18125

[56] J. H. Yoo, M. Ji, J. H. Kim, C. H. Ryu, Y. I. Lee (2020) Facile synthesis of hierarchical CuS microspheres with high visible-light-driven photocatalytic activity. Journal of Photochemistry and Photobiology A: Chemistry, 401, 112782. https://doi.org/10.1016/j.jphotochem.2020.112782

[57] M. S. Gopika, S. Jayasudha, P. B. Nair (2022) Phase transformation induced structural, optical and photocatalytic investigations of TiO2 nanoparticles. Bulletin of Materials Science, 45(2), 71. https://doi.org/10.1007/s12034-021-02647-4

[58] A. Nezamzadeh-Ejhieh N. Moazzeni (2013) Sunlight photodecolorization of a mixture of Methyl Orange and Bromocresol Green by CuS incorporated in a clinoptilolite zeolite as a heterogeneous catalyst. Journal of Industrial and Engineering Chemistry, 19(5), 1433-1442. https://doi.org/10.1016/j.jiec.2013.01.006

[59] X. Geng, Q. Feng, X. You, Q. Wang, Z. Jing (2020) A comparative study of the photocatalytic properties of CuS nanotubes and nanoparticles by hydrothermal method. Indian Journal of Chemistry-Section A (IJCA), 56(1), 57-62.DOI: 10.56042/ijca.v56i1.11529

[60] X. Deng, C. Wang, H. Yang, M. Shao, S. Zhang, X. Wang, ... X. Xu (2017) One-pot hydrothermal synthesis of CdS decorated CuS microflower-like structures for enhanced photocatalytic properties. Scientific Reports, 7(1), 3877. https://doi.org/10.1038/s41598-017-04270-y

[61] J. Zhu, Y. Zhou, W. Wu, Y. Deng, Y. Xiang, Y. Zhou (2020) Preparation of 3D flower-like Bi/CuS composite and properties of degrading dye wastewater. Journal of Materials Science: Materials in Electronics, 31, 3845-3854. https://doi.org/10.1007/s10854-020-02919-5

[62] A. Rahmani, H. Rahmani, A. Zonouzi (2017) Synthesis of copper sulfides with different morphologies in DMF and water: catalytic activity for methyl orange reduction. Materials Research Express, 4(12), 125024. https://doi.org/10.1088/2053-1591/aa9e13

IZVOD

DVOSTRUKI REŽIM ŽIVOTNE SREDINE ODRŽAVANJA TOKSIČNIH BOJA KROZ HEMO-KATALITIČKE I FOTOKATALITIČKE PUTEVE KORIŠĆENJEM KLASTERA NANOLISTOVA COVELITA (CUS)

Klasteri kovelitnih (CuS) nano listova visoke čistoće sa izuzetnim katalitičkim svojstvima sintetizovani su jednostavnim mehanohemijskim procesom, koji je efikasno rešio određene zamke tradicionalne sinteze u čvrstom stanju, uključujući višesatno mlevenje, neophodnost žarenja, da bi se uklonili nusprodukti, i prepreke u postizanju veličina kristalita ispod 20 nm. Proučavanje reakcionih mehanizama otkrilo je formiranje intermedijera [Cu(tu)] Cl. 0,5 H2O, koji je delovao kao samožrtvovani prekursor za formiranje CuS nanolistova. Opsežna karakterizacija koja uključuje XRD sa Rietveld preciziranjem, HRTEM, FESEM, EDS, UV-VIS apsorpciju, FTIR i Ramanovu spektroskopiju potvrdila je formiranje faznog čistog heksagonalnog CuS sa naslaganom morfologijom u obliku listova koji formira mikrocvetove , sa prosečnom veličinom kristalita i 11nm sa optičkim pojasom od 1,91 eV. Studije o degradaciji metil narandže (MO), glavnog zagađivača životne sredine , koristeći Covellite nan o ploče kao dvostruki katalizator , pokazale su izuzetnu efikasnost, postižući 84% degradacije za 12 minuta hemo -katalizom i 89,5% za 40 minuta fotokatalizom. Ova studija sugeriše ekološki prihvatljive i obećavajuće dvostruke puteve za eliminisanje kontaminacije organskom bojom upotrebom Covellite (CuS) nanokatalizatora.

Ključne reči: *Covellite(CuS), hemo-kataliza, fotokataliza, metilnarandža (MO), Langmuir-Hinshelvood model*

Deepthi S Nair   https://orcid.org/0009-0003-0102-6093
Jayasudha S   https://orcid.org/0009-0005-5143-847X
Ananda Kumar V M   https://orcid.org/0000-0002-7231-8056